Materials Letters 215 (2018) 15–18

Contents lists available at ScienceDirect

Materials Letters

journal homepage: www.elsevier.com/locate/mlblue

Effect of the nitrogen-argon gas mixtures on the superconductivity properties of reactively sputtered molybdenum nitride thin films

N. Haberkorn [a,b,*], S. Bengio [a], S. Suárez [a,b], P.D. Pérez [a], M. Sirena [a,b], J. Guimpel [a,b]

[a] Comisión Nacional de Energía Atómica and Consejo Nacional de Investigaciones Científicas y Técnicas, Centro Atómico Bariloche, Av. Bustillo 9500, 8400 San Carlos de Bariloche, Argentina

[b] Instituto Balseiro, Universidad Nacional de Cuyo and Comisión Nacional de Energía Atómica, Av. Bustillo 9500, 8400 San Carlos de Bariloche, Argentina

ARTICLE INFO

Article history:
Received 7 June 2017
Received in revised form 9 November 2017
Accepted 10 December 2017
Available online 11 December 2017

Keywords:
Nitrides
Sputtering
Superconductivity

ABSTRACT

We report on the superconducting properties of nanocrystalline molybdenum nitride thin films grown by reactive DC sputtering at room temperature with a N_2:Ar mixture. Thin films grown using 5% N_2 concentration display T_c = 8 K, which is gradually reduced to 5.8 K for 30% N_2 concentration, producing changes in nitrogen stoichiometry of the samples from Mo_2N to Mo_2N_{1+x} ($0 \leq x < 0.4$). The T_c is abruptly reduced and disappears for N_2 concentration between 30% and 40%, which can be attributed to an increment in the disorder due to phase coexistence between cubic γ-Mo_2N and non-superconducting amorphous MoN (dominant for N_2 concentration >40%).

1. Introduction

Transition–metal nitrides (TMN) display a wide range of electronic and mechanical properties which are promising for technological applications. Superconducting TMN are potential candidates in a wide range of cryogenic devices like tunnel junctions [1] and electromagnetic radiation detectors [2]. The Mo nitrides present several superconducting crystalline phases: γ-Mo_2N (cubic) with $T_c \sim 5$ K [3], β-Mo_2N (tetragonal) with $T_c \sim 5$ K [4] and δ-MoN (hexagonal) with $T_c \sim 12$ K [5]. Different methods have been used in the growth of Mo nitride thin films, such as reactive sputtering [6,7], pulsed laser deposition [8], thermal nitration [9] and chemical routes [10]. A distinctive feature of γ-Mo_2N thin films is the influence of the disorder on T_c, which ranges from 4.5 K to around 8 K for epitaxial and polycrystalline thin films, respectively [11,12].

In this letter, we show that the T_c in γ-Mo_2N_x thin films (grown by reactive DC sputtering at room temperature) can be tuned by modifying the N_2:Ar mixture used during the sputtering process. T_c in thin films can be modified from 8 K to temperatures below 3 K by increasing the N_2 partial pressure in the N_2:Ar mixture from 5% to 40% of the total pressure. This modification can be associated with changes in the nitrogen stoichiometry and the presence of amorphous MoN for films grown with N_2:Ar mixtures higher than 30%. Our results provide an effective and simple path to prepare Mo_2N_x thin films at room temperature with tunable T_c, which is relevant for the investigation of the fundamental properties and for technological applications (i.e. optical and electronic devices on flexible polymeric substrates) [13–15].

2. Material and methods

Mo_2N_x films were deposited by DC reactive magnetron sputtering on AlN buffered Si (0 0 1) substrates [16,17]. No intentional heating of the substrate was used. The films were obtained from a pure Mo target using 50 W in a N_2:Ar gas mixture with N_2 partial pressure going from 5% to 70% of the mixture's 5 mTorr pressure. An 8 nm thick AlN buffer layer (grown with 20% N_2 partial pressure) was introduced by RF sputtering (100 W) to avoid any chemical reaction between the Mo and the native SiO_2 layer of the Si wafers. Commercial sputtering targets with diameter of 38 mm were used. During deposition the substrate (typical size 1 cm^2) was positioned directly over the targets at ~5.5 cm. Ultra-high purity Ar (99.999%) and N_2 (99.999%) were used as gas sources. The residual pressure of the chamber was less than 10^{-6} Torr. Wherever used, the notation [MoNY%] indicates a Mo-N film grown with Y% N_2 partial pressure. The growth rate for the Mo_2N_x films is systematically reduced from ≈22 nm/min ([MoN5%]) to ≈10 nm/min ([MoN70%]).

X-ray (XRD) diffraction data were obtained using a Panalytical Empyrean equipment. The chemical composition and thicknesses

* Corresponding author at: Comisión Nacional de Energía Atómica and Consejo Nacional de Investigaciones Científicas y Técnicas, Centro Atómico Bariloche, Av. Bustillo 9500, 8400 San Carlos de Bariloche, Argentina.

E-mail address: nhaberk@cab.cnea.gov.ar (N. Haberkorn).

https://doi.org/10.1016/j.matlet.2017.12.045
0167-577X/

of the films were analyzed by Rutherford Backscattering Spectroscopy (RBS) with a TANDEM accelerator using a 2 MeV $^4He^{2+}$ ion beam. RBS spectrums were simulated with the SIMNRA code. Surface composition analysis was performed by means of X-ray photoelectron spectroscopy (XPS) using a standard Al/Mg twin-anode X-ray gun and a hemispherical electrostatic electron energy analyzer. The electrical transport measurements were performed using the standard four point configuration.

3. Results and discussion

XRD for thin films grown with N_2/Ar mixtures ≤ 40% show the 200 reflection corresponding to the cubic γ-Mo_2N structure (see Fig. 1a). The peak is systematically sifted to smaller angles for higher N_2 partial pressure, which indicates a larger lattice parameter (see Table 1). The microstructure of the films displays columnar nanometric grains (diameter smaller than 10 nm) textured along the (1 0 0) axis [16]. No X-ray reflections were identified for N_2/Ar mixtures >40%. For Mo-N films grown with different N_2 partial pressures, the electrical resistivity increases with T between 10 K and 300 K. The residual resistance ratio ($RRR = R^{300K}/R^{10K}$, with R the sample resistance) is in the range 0.96–0.6, systematically decreasing for higher N_2 partial pressures (see Table 1). This indicates a very short mean free path l due to structural disorder (grain boundaries, chemical impurities and amorphous phases). Fig. 1b shows the dependence of T_c with the N_2 partial pressure. The inset in Fig. 1b shows the temperature dependence of the normalized resistance at $T < 10$ K for the superconducting films. The results show that for [MoN5%], T_c is close to 8 K and it systematically decreases until disappearing for [MoN40%]. The superconducting transition is sharp for all samples. Considering that all the analyzed films are thicker than 40 nm, no contribution of their dimension on the T_c is expected [16]. It is important to note that epitaxial γ-Mo_2N films with $RRR \approx 50$ display T_c= 4.5 K [11] and polycrystalline γ-Mo_2N films with $RRR < 1$ display T_c = 8 K [12]. In addition, the T_c in [MoN5%] annealed up to 973 K decreases from 8 K to ≈ 5 K, which is close to the value reported for epitaxial films [11]. This indicates that for Mo-N thin films grown at room temperature the stoichiometry and the disorder are relevant parameters for T_c. Following, we will analyze the influence of the N_2:Ar mix on the chemical composition of the films using RBS and XPS. The RBS measurements show that the gradual suppression of T_c can be correlated with changes in the Mo/N chemical composition (see Fig. 1c). For [MoN5%] the stoichiometry is close to Mo_2N and it systematically decreases to MoN at [MoN40%]. MoN stoichiometry is expected for δ-MoN [10]. The absence of T_c for $N_2/(Ar + N_2) > 40\%$ could be attributed to an increment in the disorder and no crystallization of the hexagonal δ-MoN (evidenced in XRD).

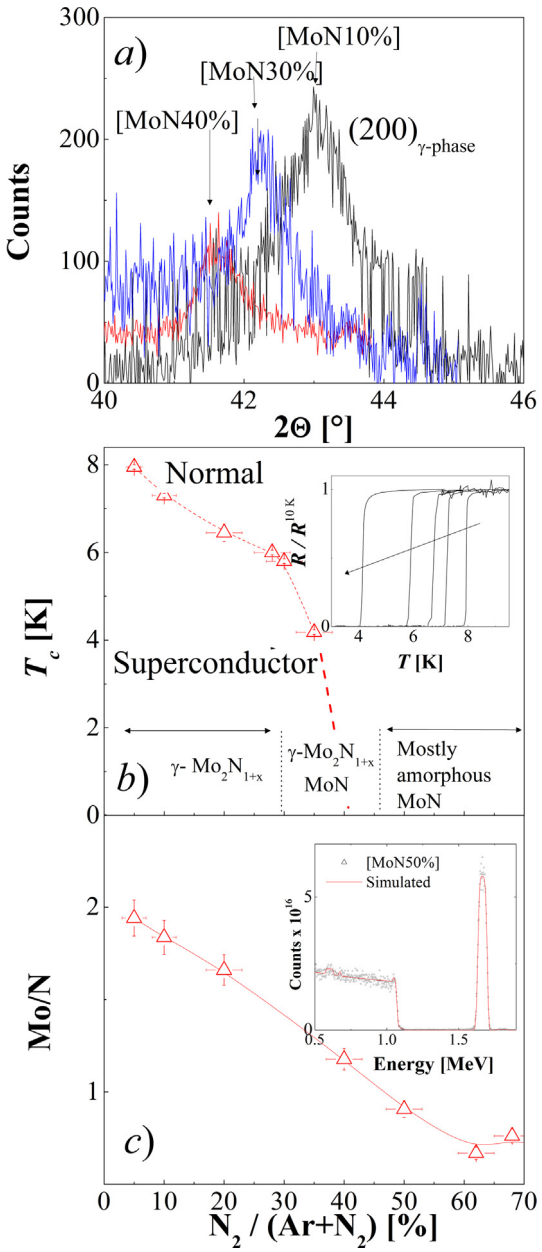

Fig. 1. Dependence with the N_2:Ar reactive gas composition for films grown in a lapse of 5 min of : a) XRD; b) T_c; c) Atomic Mo/N ratio. Inset b) Normalized resistance R/R^{10K} for the superconducting films at $T < 10$ K. The arrow indicates the change in the N_2:Ar mixture from 5% to 35%. Inset c) RBS spectra for [MoN50%].

XPS measurements were performed to obtain information of the chemical composition of the Mo-N films and the oxidation state of the Mo. The photoelectron peaks Mo3d, O1s, C1s and N1s were measured in detail. An overlapping of the N1s and Mo3p peaks was observed. The Mo3d binding energy region for each MoN film is shown in Fig. 2a–d. The spectra were fitted using a Voight function for each peak plus a Shirley-type background. The total fitted intensities along with the experimental ones are shown in each spectrum. In the [MoN10%] and [MoN20%] Mo3d spectra, up to three components were identified: a low binding energy component at 228.5 eV (which could be ascribed to $Mo^{\delta+}$ ($2 \leq \delta < 4$) associated with the compound Mo_2N [18]), an intermediate component at ≈230 eV (which could be attributed to Mo^{4+} associated to MoO_2 impurities [19]), and a high binding energy component at 232.7 eV (ascribed to the presence of Mo^{6+} due to the formation of MoO_3 in the surface [20,19]). The doublet associated to the presence of MoO_3 can be completely removed after a sputtering process, which indicates its surface nature [17]. The Mo3d spectra at [MoN10%] and [MoN20%] are dominated by $Mo^{\delta+}$. In the [MoN35%] and [MoN50%], Mo3d spectra display a new component at 229.1 eV, which can be ascribed to MoN [21]. This new component shifts the envelope of the $Mo3d_{5/2}$ peak to higher binding energy, as observed by Wang et al. [18]. From XRD, RBS and XPS data it is observed that the T_c of nanometric γ-Mo_2N_x thin films is strongly affected by the stoichiometry and the disorder. The suppression of T_c can be associated with changes in the nitrogen stoichiometry Mo_2N_{1+x} ($0 \leq x < 0.4$) ($5\% < N_2/(Ar + N_2) < 30\%$) and with an increment in the disorder due to the growth of amorphous MoN ($30\% < N_2/(Ar + N_2) < 40\%$). This is in agreement with the presence of XRD reflections corresponding to δ-MoN (hexagonal) for annealed [MoN35%] and [MoN50%] [22].

Following we analyze the upper critical field $H_{c2}(T)$ with the magnetic field perpendicular to the surface for [MoN5%],

Table 1
List of samples and related properties.

Sample	a [nm]	*RRR*	T_c [K]	H_{c2} (0) [T]	$-\delta H_{c2}/\delta t\|_{Tc}$
[MoN5%]	–	0.96	7.95 (0.05)	12.4 (0.1)	17.8 (0.1)
[MoN10%]	0.4202 (0.0005)	0.95	7.20 (0.05)	11.8 (0.1)	17 (0.2)
[MoN20%]	0.4230 (0.0005)	0.93	6.6 (0.1)	11.8 (0.1)	17 (0.2)
[MoN30%]	0.4280 (0.0005)	0.88	5.80 (0.05)	11.8 (0.1)	17 (0.2)
[MoN35%]	0.4300 (0.0005)	0.84	4.20 (0.05)	–	–
[MoN40%]	0.4330 (0.0005)	0.81	< 3	–	–
[MoN50%]	No reflections	0.8	–	–	–
[MoN60%]	No reflections	0.75	–	–	–
[MoN70%]	No reflections	0.6	–	–	–

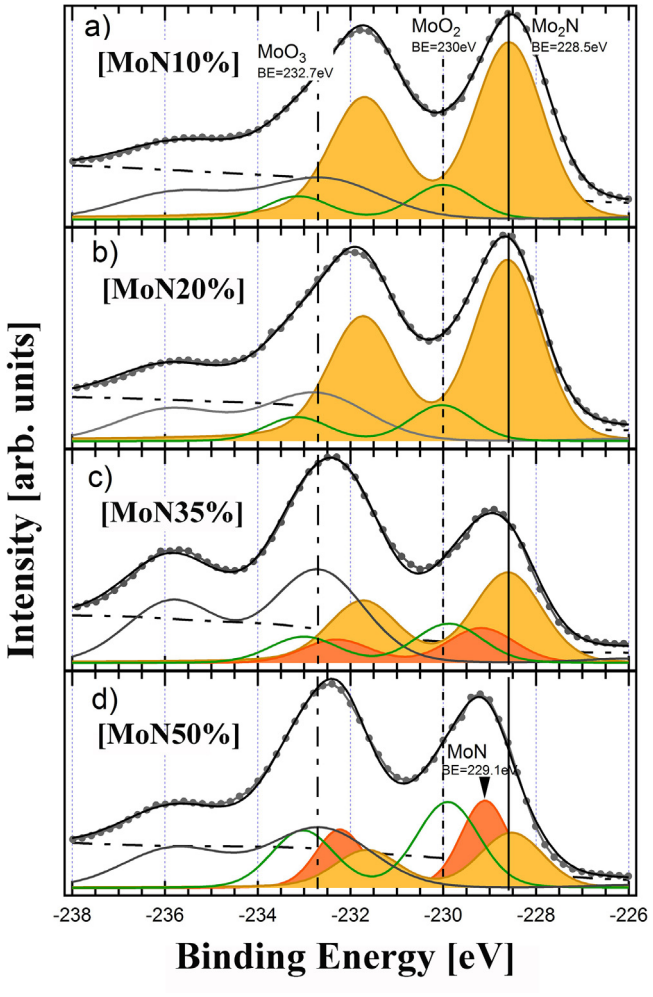

Fig. 2. XPS Mo3d spectra of: a) [MoN10%]; b) [MoN20%]; c) [MoN35%]; and d) [MoN50%].

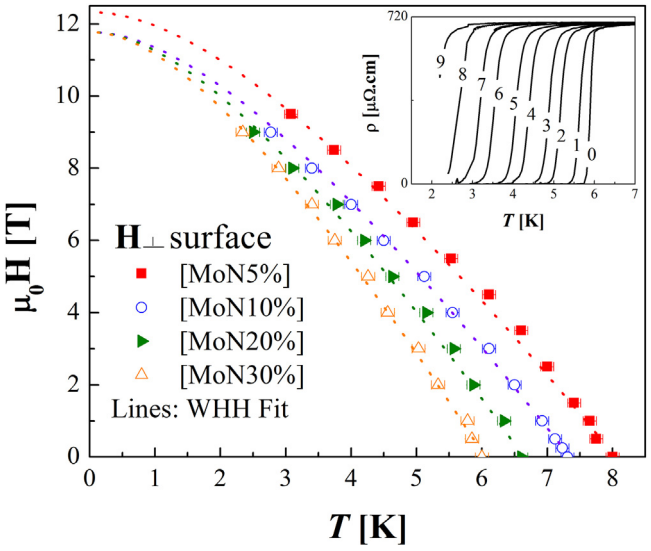

Fig. 3. Temperature dependence of the upper critical field (H_{c2}) for [MoN5%], [MoN10%], [MoN20%], and [MoN30%]. Inset: Resistivity vs. Temperature dependence for different H in [MoN30%].

[MoN10%], [MoN20%] and [MoN30%] (see Fig. 3). Inset Fig. 3 shows typical resistivity vs. temperature curves for different applied magnetic fields (H) in [MoN30%]. The temperature dependence of H_{c2} can be analyzed by the Werthamer-Helfand-Hohenberg (WHH) model developed for dirty one-band superconductors [23], which predicts

$$ln\frac{1}{t}=\sum_{v=-\infty}^{\infty}\left(\frac{1}{|2v+1|}-\left[|2v+1|+\frac{\hbar}{t}+\frac{(\alpha\hbar/t)^2}{|2v+1|+(\hbar+\lambda_{so})/t}\right]^{-1}\right) \quad (1)$$

where $t = T/T_c$, $\hbar=(4/\pi^2)(H_{c2}(T)/|dH_{c2}/dT|_{T_c})$, λ_{so} is the spin-orbit scattering constant, and α is the Maki parameter which quantifies the weakening influence of the Pauli electron spin paramagnetism on the superconducting state. When $\lambda_{so} = 0$, $H_{c2}(0)$ obtained from the WHH formula satisfies the relation $H_{c2}(0)=\frac{H_{c2}^{orb}(0)}{\sqrt{1+2}}$, which is originally derived by K. Maki [24]. All the analyzed $H_{c2}(T)$ curves followed the WHH model with $\alpha = 0$ and $\lambda_{so} = 0$. For $\alpha = 0$, $H_{c2}(T)$ is given as the pure "orbital field limit", $H_{orb}(T)$, due to the supercurrents circulating around the vortex cores. The results show that, independently of T_c, all the films present $H_{c2}(0)$ around 12 T (see Fig. 3 and Table 1). This value is close to the one expected from the Pauli limit $H_p \approx 1.84\ T_c$ [25] and corresponds to a coherence length of $\xi(0) \approx 5.2$ nm.

4. Conclusions

In summary, nanocrystalline superconducting Mo_2N_x thin films with *RRR* < 1 have been successively grown at room temperature by reactive DC magnetron sputtering. The T_c of the films can be tuned from 8 K to below 3 K by modifying the reactive $N_2/(Ar + N_2)$ composition between 5% and 40%. The drop in T_c can be attributed to changes in the Mo_2N_{1+x} ($0 \le x < 0.4$) stoichiometry ($N_2/(Ar + N_2) < 30\%$) and to an increment in the disorder produced by phase coexistence due to the growth of amorphous MoN (for $30\% < N_2/(Ar + N_2) < 40\%$). The absence of T_c for $N_2/(Ar + N_2) > 40\%$ can be related to the phase being mostly amorphous MoN.

Acknowledgments

This work was partially supported by the ANPCYT (PICT 2015-2171), U. N. de Cuyo 06/C505 and CONICET PIP 2015-0100575CO. NH, SB, MS and JG are members of the Instituto de Nanociencia y Nanotecnología (CNEA-CONICET).

References

[1] Zhen Wang et al., Appl. Phys. Lett. 75 (1999) 701–703.
[2] Chandra M. Natarajan et al., Supercond. Sci. Technol. 25 (2012), 063001-063001(16).
[3] B.T. Matthias, J.K. Hulm, Phys. Rev. 87 (1952) 799–806.
[4] Kei Inumaru et al., Chem. Mater. 17 (2005) 5935–5940.
[5] Shanmin Wang et al., Sci. Rep. 5 (2015), 13733-13733(8).
[6] Y.H. Shi et al., Phys. Rev. B 38 (1988) 4488–4491.
[7] H. Ihara et al., Phys. Rev. B 32 (1985) 1816–1817.
[8] Kei Inumaru et al., Phys. Rev. B 73 (2006), 52504-52504(4).
[9] D.K. Christen et al., IEEE Trans. Magn. 23 (1987) 1014–1018.
[10] Y.Y. Zhang et al., J. Am. Chem. Soc. 133 (2011) 20735–20737.
[11] Hongmei Luo et al., J. Phys. Chem. C 115 (2011) 17880–17883.
[12] R. Baskaran et al., J. Phys. D 49 (2016) 205304–205307.
[13] E. Rudenko et al., J. Appl. Phys. 121 (2017) 135304.
[14] Dongping Zhang et al., Appl. Phys. A 97 (2009) 437–441.
[15] Flora M. Li et al., Thin Solid Films 520 (2011) 1278–1284.
[16] W.D. Sproul et al., Thin Solid Films 491 (2005) 1–17.
[17] N. Haberkorn et al., Mater. Chem. Phys. 204 (2018) 48–57.
[18] Y.M. Wang, R.Y. Lin, Mater. Sci. Eng. B 112 (2004) 42–49.
[19] Z.B. Zhaobin Wei, P. Grange, B. Delmon, Appl. Surf. Sci. 135 (1998) 107–114.
[20] G.-T. Kim et al., Appl. Surf. Sci. 152 (1999) 35–43.
[21] Kejun Zhang et al., Appl. Mater. Interfaces 5 (2013) 3677–3682.
[22] N. Haberkorn, et al. (unpublished).
[23] N.R. Werthamer, E. Helfand, P.C. Hohenberg, Phys. Rev. 147 (1966) 295–302.
[24] K. Maki, Phys. Rev. 148 (1966) 362–369.
[25] M. Tinkham, Introduction to Superconductivity, second ed., McGraw-Hill, 1996.